

Article

Breaking Down SERS Detection Limit: Engineering of a Nanoporous Platform for High Sensing and Technology

Federico Scaglione , Livio Battezzati  and Paola Rizzi 

Dipartimento di Chimica and Centro Interdipartimentale NIS (Nanostructured Interfaces and Surfaces), Università di Torino, V. Giuria 7, 10125 Turin, Italy; livio.battezzati@unito.it (L.B.); paola.rizzi@unito.it (P.R.)

* Correspondence: federico.scaglione@unito.it

Abstract: In this study, nanoporous gold (NPG) was synthesized by free corrosion dealloying of an amorphous precursor, $\text{Au}_{20}\text{Cu}_{48}\text{Ag}_7\text{Pd}_5\text{Si}_{20}$ (at. %), in a mixture of nitric and hydrofluoric acid, starting from amorphous melt-spun ribbons. NPG revealed a 3D nanoporous structure composed of pores and multigrain ligaments of an average size of 60 nm. NPG was further anodized in oxalic acid at 8 V vs. Ag/AgCl reference electrode to obtain a bimodal morphology composed of ligaments disrupted in finer features. Both NPG and anodized samples (A-NPG) were found to be mechanically stable to bending and active for surface-enhanced Raman scattering (SERS). SERS activity of samples was investigated using 4,4'-bipyridine as a probe molecule. A detection limit of 10^{-16} M was found for both samples, but in A-NPG, the signal was strongly enhanced. The extremely high enhancement obtained for A-NPG is attributed both to the small size of ligaments and crystals of which they are made, as well as to the nanometric features resulting from anodization treatment. Such a microstructure showed homogenous SERS response in terms of average enhancement all across the surface, as demonstrated by mapping measurements. Furthermore, NPG and A-NPG were tested as electrodes for electrocatalytic applications, showing good properties. The engineering steps from the amorphous precursor to A-NPG led us to obtain a high-sensing platform, with extremely low detection limit and intrinsic properties, that might significantly contribute to the cutting-edge technology of the future.

Keywords: nanoporous gold; anodization; chemical dealloying; amorphous precursor; SERS; electrocatalyst



Citation: Scaglione, F.; Battezzati, L.; Rizzi, P. Breaking Down SERS Detection Limit: Engineering of a Nanoporous Platform for High Sensing and Technology. *Nanomaterials* **2022**, *12*, 1737. <https://doi.org/10.3390/nano12101737>

Academic Editors: Gerard Tobias, Stefania Sandoval and Hui-Fen Wu

Received: 21 March 2022

Accepted: 17 May 2022

Published: 19 May 2022

Publisher's Note: MDPI stays neutral with regard to jurisdictional claims in published maps and institutional affiliations.



Copyright: © 2022 by the authors. Licensee MDPI, Basel, Switzerland. This article is an open access article distributed under the terms and conditions of the Creative Commons Attribution (CC BY) license (<https://creativecommons.org/licenses/by/4.0/>).

1. Introduction

Studies on nanostructured materials are progressively increasing year by year, due to their unique properties, completely different from those of their bulk counterparts.

In particular, nanoporous metals prepared by dealloying techniques have been receiving research interest and exhibit promising results in several fields of application: actuators [1], storage and conversion of energy [2], electrodes for electrocatalysis [3,4], electrochemical biosensors [5–7], and surface-enhanced Raman scattering [8,9]. Scattering enhancement has been ascribed to their high surface area and their morphology constituted in ligaments, ranging from tens to hundreds of nanometers, and basically composed of the noblest elements of the original alloy. Dimensions of pores and ligaments can be tuned by selecting a proper alloy composition and changing dealloying parameters [10]. Furthermore, previous studies demonstrated how the original structure of the precursor, i.e., crystalline or amorphous, affects the morphology and microstructure of ligaments and related properties. When a crystalline alloy is dealloyed, the nanoporous material that is formed retains the crystal structure of the precursor: Lesser noble elements are dissolved into the electrolyte, while the nobler element diffuses by surface diffusion forming ligaments with a smooth appearance [11]. In the case of an amorphous precursor, ligaments are made up of many nanocrystals [12] originated by the germination during the transition from amorphous to crystalline structure [13,14]: When lesser noble atoms

of the amorphous alloy are dissolved in the electrolyte, more noble atoms are freed by lateral coordination and move as ad-atoms by surface diffusion forming clusters that grow in dimension with the proceeding of the process until they impinge together forming ligaments. As a result, ligaments obtained from the dealloying of an amorphous precursor are multigrained, with more active sites at the grain boundaries and defects, making them more favorable in electrocatalysis applications [15–17] and surface-enhanced Raman spectroscopy (SERS) [18].

SERS is a technique based on the enhancement of light Raman scattering of molecules adsorbed on plasmonic metallic nanostructures [19,20]; nanostructures can be self-standing or supported on oxides as in the case of metallic nanoparticles [21]. The SERS activity of different substrates can be compared according to the enhancement factor (EF), which, consequently, may affect the limit of detection (LOD), i.e., the lowest amount or concentration detectable on the substrate for a given analyte [22]. EF changes by different orders of magnitude depending on the interaction between substrate and molecules (chemical enhancement) and on the nanostructured surface (electromagnetic field enhancement): The former can result in an EF change of two orders of magnitude [23,24], while the latter arises from the resonant excitation of localized surface plasmons on the metallic surface and dramatically raises the EF [25]. The electromagnetic field enhancement is strongly connected to specific features and dimensions of the nanostructures, i.e., sharp edges and tips [26], interparticle gaps [27], and nanopores [28], typically defined as “hot spots”. Due to this behavior, SERS represents a sensitive technique to reveal molecules of analyte in low quantities that can be improved through the optimization of metallic nanostructured substrates.

In the frame of this application, in this study, a sensor–substrate platform for SERS was investigated, which was obtained by dealloying an $\text{Au}_{20}\text{Cu}_{48}\text{Ag}_7\text{Pd}_5\text{Si}_{20}$ amorphous ribbon. The resulting nanoporous gold (NPG) was then electrochemically treated via anodization, forming tiny features on NPG ligaments: The final sample was constituted by anodized nanoporous gold (A-NPG) and exhibited a higher SERS activity, as it was able to reveal probe molecules in extremely low concentration, i.e., 10^{-16} M with 4-4' bipyridine. Once the extremely high SERS activity of the A-NPG sample was proven with a probe molecule, measurements were provided with a molecule of interest whose affinity with the substrate was considered weaker than previous probe molecules: Ascorbic acid was selected due to the need for measuring this molecule in a very low concentration since it is involved in several biological processes or widely used in the pharmaceutical field and in the food industry as a nutritional supplement and food preservative. Furthermore, since the samples were both NPG and A-NPGs self-standing materials, these samples were successfully tested as electrodes for electrocatalytic applications using the same molecule.

2. Materials and Methods

Lumps of pure elements (Au: 99.99%, Si: 99.9995%, Ag, Cu, Pd: 99.99%) were arc-melted in a Ti-gettered Ar atmosphere to obtain a master alloy ingot of composition $\text{Au}_{20}\text{Cu}_{48}\text{Ag}_7\text{Pd}_5\text{Si}_{20}$ (at. %). The ingot was then placed in a quartz crucible, melted via induction, and rapidly quenched via the melt-spinning technique; the rapid solidification process consists of spinning the molten alloy onto a copper wheel, rotating at a speed rate of 25 m/s. The heat of the molten alloy is rapidly dissipated by the wheel, and solidification occurs in form of ribbons, skipping crystallization. Ribbons were 2 mm wide, 20–25 μm thick, and appeared to be fully amorphous according to the X-ray diffraction (XRD) analysis. Dealloying of ribbons was performed by chemical means in a mixture of 10 M HNO_3 + 0.5 M HF at 70 °C for 4 h; HF was added to avoid the formation of SiO_2 when the contained silicon in the alloy precursor is oxidized. These conditions were optimized in our previous research to obtain the desired NPG morphology [29]. Pieces of NPG ribbon, 3 cm in length, were subsequently anodized in 0.3 M oxalic acid solution while applying a potential of 8 V for 3, 5, and 7 min. Samples were used as working electrodes in a cell composed of an Ag/AgCl reference electrode in a double-bridge configuration and a Pt-grid counter electrode.

As prepared ribbons, NPG and anodized samples (A-NPG) were properly characterized. The microstructure and structure of dealloyed samples were studied via scanning electron microscopy (SEM) with energy-dispersive X-ray spectroscopy (EDS) after Co calibration and X-ray diffraction (XRD) in Bragg–Brentano geometry with Cu-K α radiation. Ligaments' size was measured at their narrower necks using Leica software [30]. All samples were deeply rinsed with ultrapure water to remove the excess acid solution inside pores and then air-dried before electrochemical or SERS experiments.

Electrocatalytic properties toward oxidation of ascorbic acid (AA) were studied using the same experimental setup as that applied for anodization. A buffer solution of 0.1 M KH₂PO₄ with 0.02 M ascorbic acid was used as the electrolyte. Current densities have been normalized by making use of the electrochemically active surface area of the electrode [31,32]. Micro-Raman measurements were performed with a Renishaw inVia Raman Microscope using a 785 nm laser line with an acquisition time of 20 s, an accumulation of 10 spectra, 0.05% power at the sample, and a 50 \times objective; 4,4'-bipyridine was chosen as probe molecules for SERS experiments.

NPG and A-NPG samples were immersed in an ethanol solution of 4,4'-bipyridine with a concentration from 10⁻¹⁶ M to 10⁻¹² M overnight, enabling the probe molecules to be adsorbed on the surface. Measurements were performed on the sample after drying in air, acquiring random spots on the surface or maps in contiguous areas. SERS intensity mapping image of a 20 \times 24 μm^2 area with a step length of 2 μm was collected using a 4,4'-bipyridine concentration of 10⁻¹² M through monitoring the characteristic peak of the probe molecule at 1619 cm⁻¹. All solutions were prepared from chemical-grade reagents and deionized water. The spectrometer was calibrated before measurements using the Raman band of a silicon wafer at 520 cm⁻¹.

3. Results and Discussion

The engineering steps to synthesize the A-NPG platform are reported as follows (the step procedure is schematized in Figure 1): NPG was obtained by free dealloying of the amorphous precursor in 10 M HNO₃ + 0.5 M HF at 70 °C for 4 h; then, it was anodized in 0.3 M oxalic acid solution applying a potential of 8 V (vs. Ag/AgCl) for different times. In what follows, the full characterization of NPG and A-NPG samples is reported.

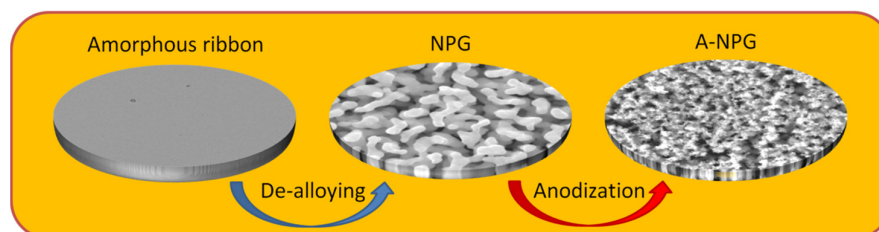


Figure 1. Engineering step procedure for A-NPG: the amorphous ribbon is dealloyed to obtain NPG. Then, anodization of NPG in 0.3 M oxalic acid solution leads to anodized NPG.

3.1. Morphology Evolution during Anodization Treatment

After dealloying, the nanoporous structure presented as a network of ligaments and pores spread over the whole thickness of the ribbon (Figure 2a,b,i). The average size of ligaments was evaluated as 60 nm, measured on the ligament's neck. Ligaments are polycrystalline, with grain boundaries joining different crystals, as evidenced by dot lines in the inset of Figure 2b; such a morphology results during the dealloying of an amorphous precursor [14], where the mechanism of dissolution of the lesser noble elements and diffusion of the noble one creates gold nanocrystals impinged together, forming ligaments. After 3 min of anodization, the A-NPG sample showed (Figure 2c,d and inset) an increased roughness constituted by asperities and features (less than 10 nm) randomly formed on the surface during the treatment.

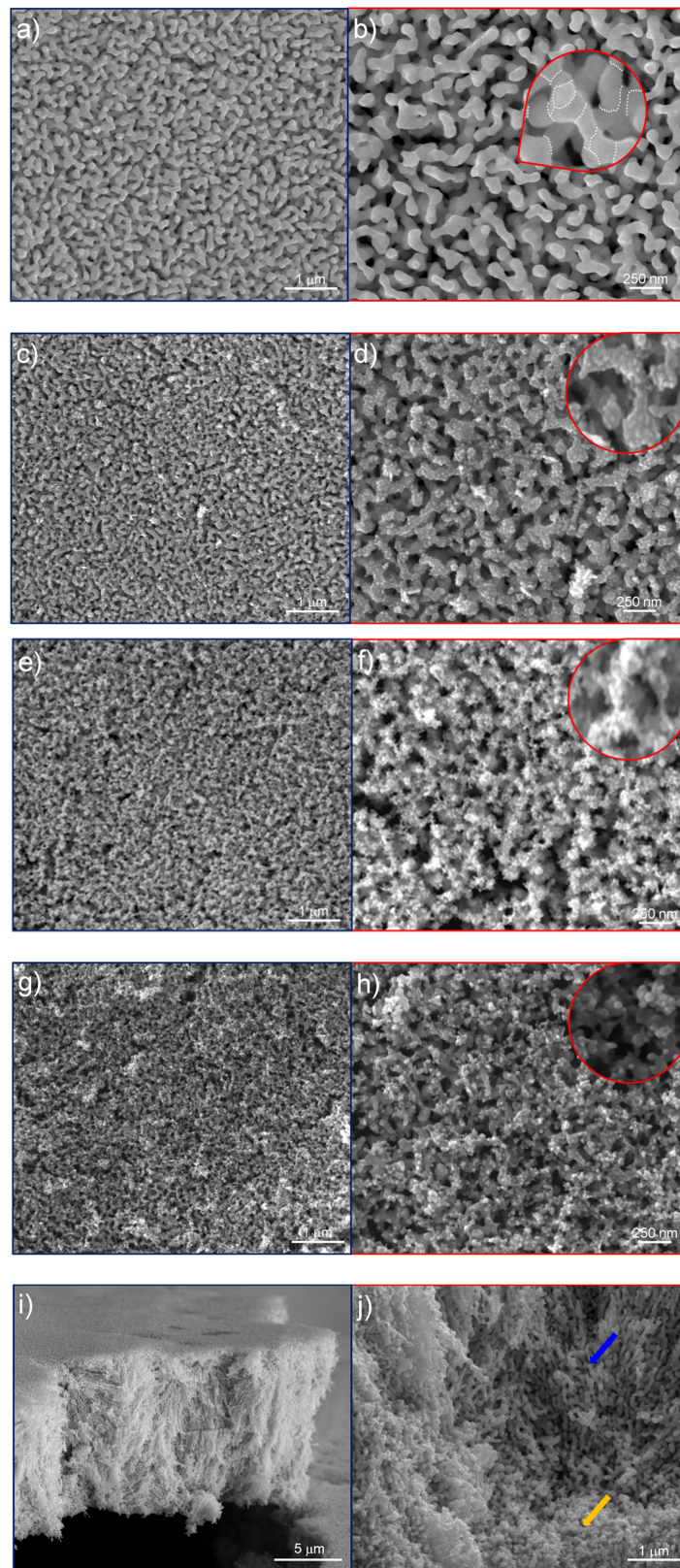


Figure 2. SEM images of the surface of samples: (a,b) NPG; (c,d) 3 min A-NPG; (e,f) 5 min A-NPG; (g,h) 7 min A-NPG. In these insets, an increased level of detail of ligaments is shown; (i) cross-sectional view of NPG; (j) cross-sectional view of the 5 min A-NPG. Anodization involved only a few microns on the nanoporous structure inside the thickness of the ribbon (yellow arrow); the inner part of the ribbon was indeed untouched by the treatment (blue arrow).

In the sample anodized for 5 min (5 min A-NPG), the roughness evolved in several pointed regions and tips of roughly 10 nm (Figure 2e,f and inset). After increasing the time of anodization to 7 min, the roughness seemed to be reduced in smoothed particles ranging from 20 to 40 nm in size (Figure 2g,h and inset).

The cross-sectional view for anodized samples (Figure 2j) displayed a morphology in the external part of the ribbon that was affected by the anodization treatment (see yellow arrow), whereas when observing the inside of the section thickness, the NPG morphology was maintained (see blue arrow). EDS analyses performed on NPG samples showed that ligaments were composed of almost pure gold (96.9 at. %), with impurities of copper (0.3 at. %), silver (1.2 at. %), silicon (1.5 at. %), and palladium (0.1 at. %) as remains of the dealloying process. As reported elsewhere [33], retained atoms, silver, in particular, are supposed to contribute to the SERS enhancement.

During anodization, the NPG surface undergoes electro-oxidation [34]; however, this gold oxide is easily reduced to zero-valent gold by oxalic acid, as reported elsewhere [35].

XRD patterns of the as-spun ribbon, NPG, and 3 min A-NPG are reported in Figure 3. The amorphous halo of the precursor disappeared after the full dealloying of the ribbon, while reflections of the Au fcc increased in the NPG pattern. As expected, the pattern of the 3 min A-NPG sample did not show significant differences from that of the previous one.

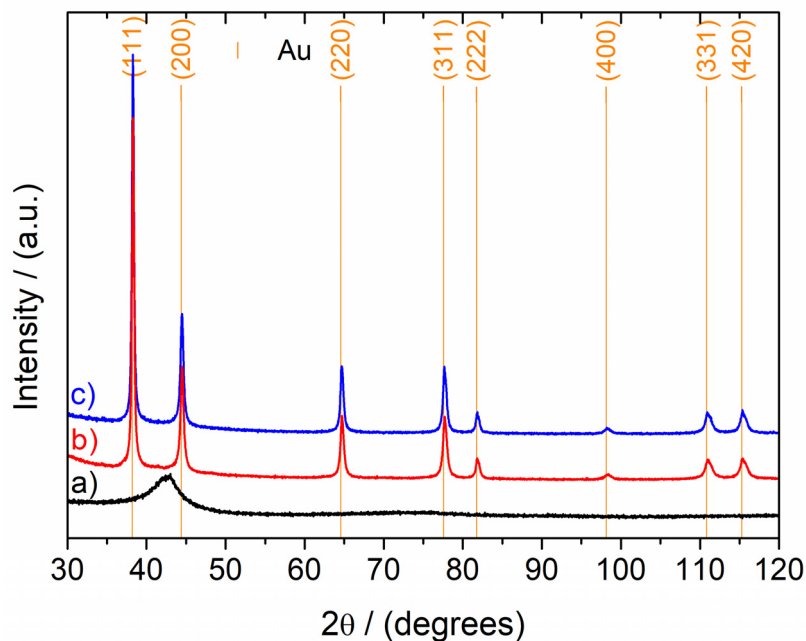


Figure 3. XRD patterns of the as-spun ribbon, NPG, and 3 min A-NPG. The amorphous halo of the as-quenched ribbon (a) disappeared after dealloying treatment, while Au fcc reflections appeared on the NPG (b) and A-NPG (c) patterns.

3.2. Mechanical Stability and Electrocatalytic Properties

NPG and A-NPG present unique hallmarks with respect to the SERS substrates currently on the market (Ocean Optics [36], Hamamatsu [37]).

Commercial substrates are categorized into two groups: patterned, metallic nanostructures formed by nanoimprint and laser technology, and metallic (Au, Ag) nanoparticles supported by oxides. Both are assembled on a handling plate material of larger dimensions relative to the active area, which limits their versatility of use.

NPG and A-NPG are self-standing, mechanically stable, and flexible if handled with laboratory tweezers; this makes the integration of the substrate into a handling plate unnecessary, widening their range of application in different operative conditions. The flexibility and bendability of samples can be observed in photos shown in Figure S1, Supplementary Materials.

Indeed, the ribbon shape makes them extremely practical for solution measurements, at air after incubation, and in the cuvette. As electrodes, NPG and A-NPG take advantage of the mechanical stability and can be incorporated into sensors and small devices. Another important aspect concerns the possibility to reuse the substrate, something not ever foreseen by other substrates on the market. In fact, NPG can be reused up to twenty times [5] and A-NPG twice, keeping its sensitivity unchanged after washing in piranha solution (70% sulfuric acid, 30% hydrogen peroxide) and abundant rinsing in deionized water until neutrality.

Electrocatalytic properties were studied in the case of the electrochemical oxidation of ascorbic acid (AA) using A-NPG as a working electrode in a cell composed of a Pt counter electrode and a saturated Ag/AgCl reference electrode in a double-bridge configuration. A buffer solution of 0.1 M KH_2PO_4 with 0.02 M ascorbic acid was used as the electrolyte. In Figure 4, CV scans at different scan speeds are reported. The oxidative current of the AA increases as a function of the scan speed due to the heterogeneity of the system. Plotting the intensity of the current density vs. the scan speed, both on a logarithmic scale, revealed a linear trend (Figure 4b), suggesting that the process is under diffusive control [38]. Similar results were obtained with NPG, in the same experimental conditions. Furthermore, in that case, a calibration line was obtained by scanning the electrode in the same buffer solution but at different concentrations of AA. Then, the capability of the electrode was verified in the determination of the analyte in a real sample; a Cebion Vitamin C Orange Effervescent tablet of 1000 mg AA (Bracco) was directly dissolved in a proper amount of buffer solution. The oxidative current density registered in such a solution was reported in terms of concentration, followed by grams per tablet of analyte; owing to the former calibration line, recovery concentration and grams content were in good agreement with the package leaflet.

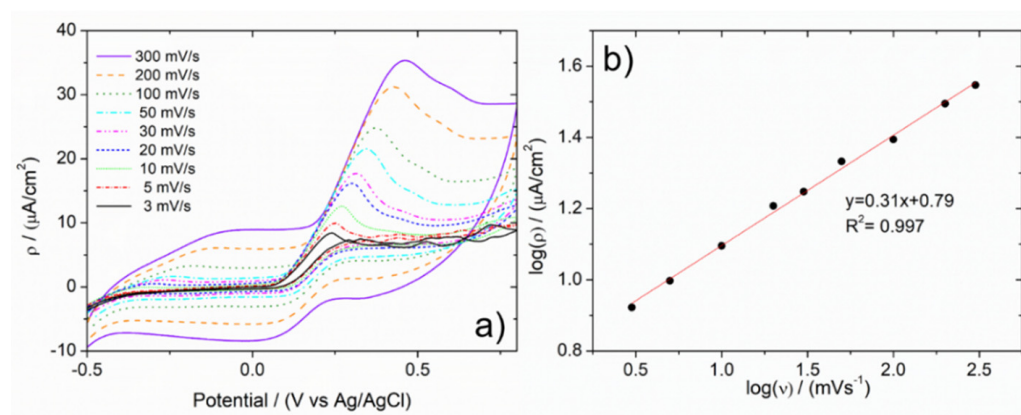


Figure 4. (a) CV scans of 0.02 M ascorbic acid in 0.1 M KH_2PO_4 solution at 3 min A-NPG electrode as a function of scan speed; (b) plot $\log(\rho)$ vs. $\log(v)$ showing linearity trend and diffusive control process.

3.3. SERS Activity

SERS activities of NPG and A-NPG were measured by dipping samples in 4-4'-bipyridine ethanol solution in diluted concentration (i.e., 10^{-12} M, 10^{-14} M, 10^{-16} M). Figure 5a–d shows the highest spectra collected for NPG, 3 min A-NPG, 5 min A-NPG, and 7 min A-NPG, respectively. Spectra show the main signals attributed to the molecule in agreement with the literature [39,40]. The enhancement of the signal was observed in all samples, but it strongly improved, especially at 10^{-16} M, in the 3 min A-NPG sample: the average intensity of the signal as a function of bipyridine concentration was 11 times higher, compared with the one of the NPG sample. This value is extremely interesting, considering that SERS substrates currently on the market (i.e., supported Au/Ag nanoparticles, lithographed Au) report a detection limit in the ppm–ppb range, using probe molecules; therefore, no more than 10^{-9} M and five orders of magnitude smaller than 10^{-16} M was

obtained with 3 min A-NPG sample. A stronger signal when the concentration is lower might be assigned to a hot spot, which is randomly distributed and located on the surface.

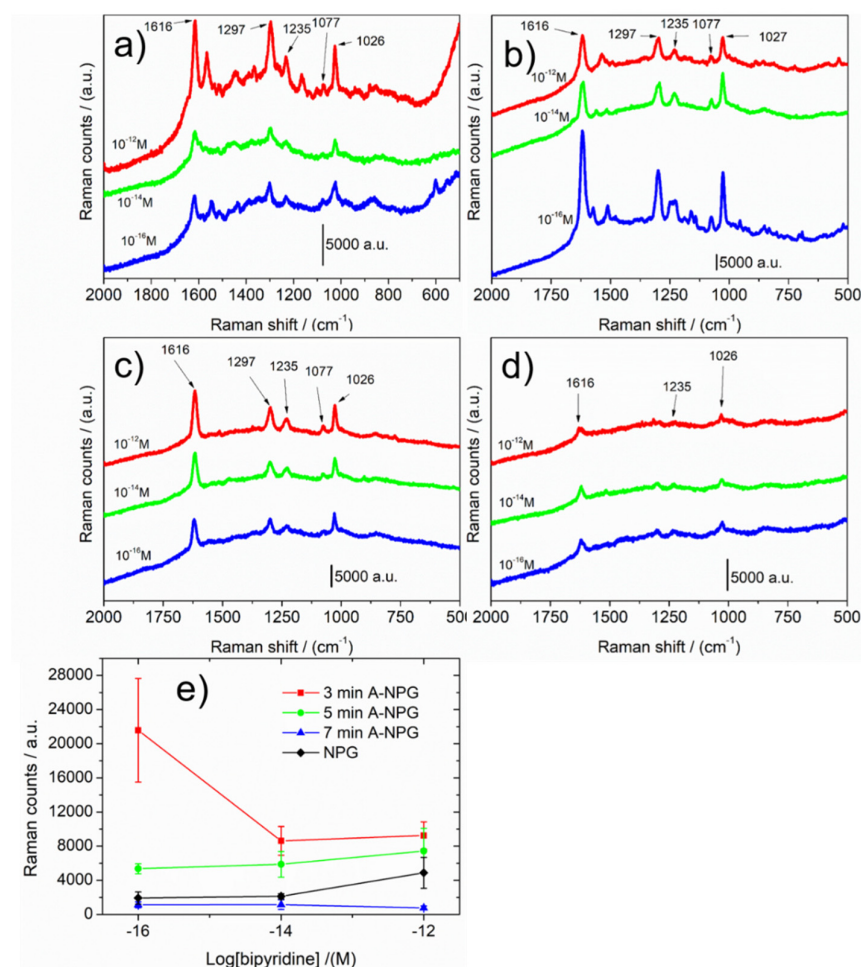


Figure 5. The highest SERS spectra (average of 10 accumulations) of 4,4'-bipyridine at different concentrations on (a) NPG, (b) 3 min A-NPG, (c) 5 min A-NPG, and (d) 7 min A-NPG; (e) Raman intensity at 1616 cm⁻¹ versus bipyridine concentrations (on logarithmic scale). The error bars were calculated from at least five measurements on random spots on the same substrate.

In the literature, a similar detection limit is reported with rhodamine 6G as a probe molecule, on complex structures constituted by silver nanoparticles decorated with zinc oxide/silicon heterostructured arrays [41] or three-dimensional sunflower-like nanoarrays decorated with Ag nanoparticles [42]. However, their expensive and time-consuming methods of preparation represent a significant drawback for large-scale applications.

The higher sensibility of A-NPGs is due to the finer double-nanostructured morphology of samples: ligaments of 60 nm with smaller features obtained by the anodization treatment. Researchers believe that the plasmonic effect of nanostructured metallic surfaces is divided into two contributions—the chemical enhancement due to the charge transfer between adsorbed molecules and substrate and electromagnetic enhancement due to the morphology and microstructure of the substrate. Considering that the former contributes two orders of magnitude to the whole enhancement, the latter contributes considerably, demonstrating the higher sensibility of the A-NPG. The enhancement factor (EF) of NPG, 3 min A-NPG, 5 min A-NPG, and 7 min A-NPG was calculated according to the calculation formula of [43] as 2×10^{13} , 1×10^{17} , 3×10^{16} , and 6×10^{15} , respectively.

Figure 6a,b report SERS intensity mapping images with bipyridine concentration of 10⁻¹² M on NPG and 3 min A-NPG, respectively. The intensity of the signal was not constant along the surface due to the presence of “hot spots” distributed at random (red

regions of the maps). As already observed in a previous study [44], the spot-to-spot intensity variation can be attributed to the localized variation of the electromagnetic field at each “hot spot”, as well as the dynamics and unique environment of a single molecule [26].

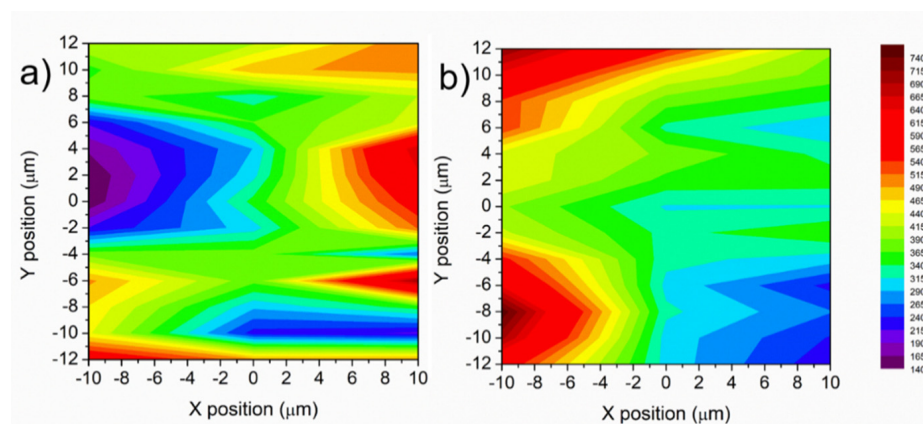


Figure 6. SERS intensity map image of $20 \times 24 \mu\text{m}^2$ by lateral step of $2 \mu\text{m}$ with 4-4' bipyridine concentration of 10^{-12}M based on characteristic peak at 1616cm^{-1} on (a) NPG and (b) 3 min A-NPG. The reader is referred to the web version of this article for interpretation of the references to color in this figure legend.

However, in the 3 min A-NPG, the average intensity was more shifted in the yellow-red intensity scale bar (Figure 6b), meaning a general sensing improvement of the substrate after anodization.

Detection of molecules of interest was successfully attempted for NPG with melamine approaching a detection limit of 10^{-6}M [29]. In Figure 7, the SERS activity of 3 min A-NPG tested in ascorbic acid aqueous solution is reported; a LOD of 10^{-3}M was measured for the anodized sample, while NPG did not show any interaction with the analyte and the spectrum, not reported, is a flat line. This further confirmed the higher sensitivity of the A-NPG sample.

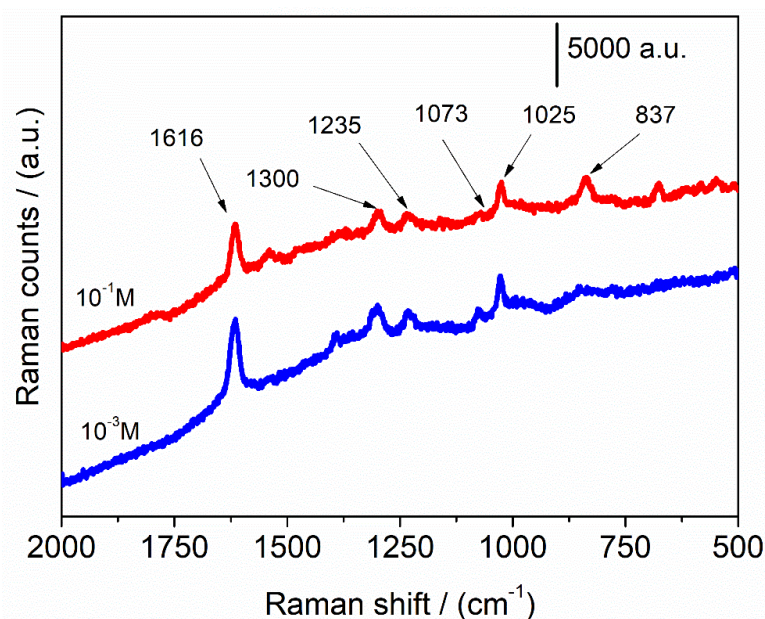


Figure 7. The highest SERS spectra (average of 10 accumulations) of ascorbic acid at different concentrations on 3 min A-NPG. Spectra were acquired randomly on the surface.

4. Conclusions

A nanoporous gold obtained by free dealloying of an amorphous precursor was successfully anodized in 0.3 M oxalic acid solution at 8 V (vs. Ag/AgCl) for different times. The ligament morphology evolved from the NPG sample to the A-NPG, increasing the roughness and forming asperities and tips as a function of the time: after three minutes of anodization, roughness and features 5–10 nm in size were formed on ligaments; in contrast, when the treatment was prolonged for 7 min, a smoothening effect prevailed, and roundish smoothed particles of 20–40 nm in size were formed.

NPG and A-NPG samples result in an easy-to-handle, self-standing material, well-suited as an electrode for electrocatalysis and substrate for SERS.

Electrocatalytic performances were proved by studying the electro-oxidation of ascorbic acid in a buffer solution: CV scan plots showed a signal associated with the oxidative current density of the analyte, increasing as a function of the scan speed and suggesting that the process was under diffusive control.

SERS activity was attempted first with a probe molecule, 4-4' bipyridine, reaching a LOD of 10^{-16} M, and for 3 min A-NPG sample, an intensity 11 times higher compared with that of the NPG. Higher activity of 3 min A-NPG was ascribed to the localized enhanced electromagnetic fields at nanosized ligaments and features obtained after anodization. A trial with ascorbic acid in an aqueous solution showed a SERS signal of the molecule down to 10^{-3} M. These results revealed that this anodized nanoporous gold can be successfully applied as an ultrasensitive sensor–substrate platform for SERS and as an electrode for catalysis or chemical and biological analyses.

5. Patents

This paper is based on the in-print Italian patent number 102020000024382 filed on 15 October 2020 and patent number PCT/IB2021/059525 filed on 15 October 2021 [45,46].

Supplementary Materials: The following supporting information can be downloaded at: <https://www.mdpi.com/article/10.3390/nano12101737/s1>, Figure S1: Photo of 3 min A-NPG bent and kept with tweezers. A-NPG is mechanically stable.

Author Contributions: Conceptualization, F.S.; methodology, F.S.; validation, F.S.; formal analysis, F.S.; investigation, F.S.; resources, P.R. and L.B.; data curation, F.S.; writing—original draft preparation, F.S.; writing—review and editing, F.S, L.B. and P.R.; visualization, F.S.; supervision, L.B. and P.R.; project administration, P.R. and L.B.; funding acquisition, P.R. and L.B. All authors have read and agreed to the published version of the manuscript.

Funding: This research was supported by the funding scheme of the European Commission, Marie Curie Actions-Initial Training Networks (ITN) in the frame of the project VitriMetTech-Vitrified Metals Technologies and Applications in Devices and Chemistry, 607080 FP7-PEOPLE-2013-ITN and by BINGO Project–Torino_call2014_L2_146 and Bando ex-post 2018 supported by Fondazione Compagnia di San Paolo Italy.

Data Availability Statement: The raw/processed data required to reproduce these findings cannot be shared at this time, as the data also form part of an ongoing study.

Conflicts of Interest: The authors declare no conflict of interest.

References

1. Ye, X.-L.; Jin, H.-J. Sealing-Free Fast-Response Paraffin/Nanoporous Gold Hybrid Actuator. *Nanotechnology* **2017**, *28*, 385501. [CrossRef] [PubMed]
2. Li, R.; Liu, X.; Wang, H.; Wu, Y.; Lu, Z.P. Development of Electrochemical Supercapacitors with Uniform Nanoporous Silver Network. *Electrochim. Acta* **2015**, *182*, 224–229. [CrossRef]
3. Fujita, T.; Guan, P.; McKenna, K.; Lang, X.; Hirata, A.; Zhang, L.; Tokunaga, T.; Arai, S.; Yamamoto, Y.; Tanaka, N.; et al. Atomic Origins of the High Catalytic Activity of Nanoporous Gold. *Nat. Mater.* **2012**, *11*, 775–780. [CrossRef] [PubMed]
4. Raj, D.; Scaglione, F.; Fiore, G.; Celegato, F.; Rizzi, P. Nanostructured Molybdenum Oxides from Aluminium-Based Intermetallic Compound: Synthesis and Application in Hydrogen Evolution Reaction. *Nanomaterials* **2021**, *11*, 1313. [CrossRef] [PubMed]

5. Scaglione, F.; Alladio, E.; Damin, A.; Turci, F.; Baggiani, C.; Giovannoli, C.; Bordiga, S.; Battezzati, L.; Rizzi, P. Functionalized Nanoporous Gold as a New Biosensor Platform for Ultra-Low Quantitative Detection of Human Serum Albumin. *Sens. Actuators B Chem.* **2019**, *288*, 460–468. [[CrossRef](#)]
6. Yang, C.L.; Zhang, X.H.; Lan, G.; Chen, L.Y.; Chen, M.W.; Zeng, Y.Q.; Jiang, J.Q. Pd-Based Nanoporous Metals for Enzyme-Free Electrochemical Glucose Sensors. *Chin. Chem. Lett.* **2014**, *25*, 496–500. [[CrossRef](#)]
7. Xue, Y.; Wang, S.; Shi, P.; Huang, Y.; Scaglione, F.; Rizzi, P.; Battezzati, L.; Denis, P.; Fecht, H.J. Nanoporous Gold Chemically De-Alloyed from Au-Based Amorphous Thin Film for Electrochemical Nonenzymatic H₂O₂ Sensing. *Chem. Phys. Lett.* **2019**, *723*, 22–27. [[CrossRef](#)]
8. Xue, Y.; Scaglione, F.; Rizzi, P.; Battezzati, L. Improving the Chemical De-Alloying of Amorphous Au Alloys. *Corros. Sci.* **2017**, *127*, 141–146. [[CrossRef](#)]
9. Xue, Y.; Scaglione, F.; Celegato, F.; Denis, P.; Fecht, H.-J.; Rizzi, P.; Battezzati, L. Shape Controlled Gold Nanostructures on De-Alloyed Nanoporous Gold with Excellent SERS Performance. *Chem. Phys. Lett.* **2018**, *709*, 46–51. [[CrossRef](#)]
10. Rizzi, P.; Scaglione, F.; Battezzati, L. Nanoporous Gold by Dealloying of an Amorphous Precursor. *J. Alloys Compd.* **2014**, *586*, S117–S120. [[CrossRef](#)]
11. Van Petegem, S.; Brandstetter, S.; Maass, R.; Hodge, A.M.; El-Dasher, B.S.; Biener, J.; Schmitt, B.; Borca, C.; Swygenhoven, H. Van on the Microstructure of Nanoporous Gold: An X-Ray Diffraction Study. *Nano Lett.* **2009**, *9*, 1158–1163. [[CrossRef](#)] [[PubMed](#)]
12. Yu, J.; Ding, Y.; Xu, C.; Inoue, A.; Sakurai, T.; Chen, M. Nanoporous Metals by Dealloying Multicomponent Metallic Glasses. *Chem. Mater.* **2008**, *20*, 4548–4550. [[CrossRef](#)]
13. Paschalidou, E.M.; Celegato, F.; Scaglione, F.; Rizzi, P.; Battezzati, L.; Gebert, A.; Oswald, S.; Wolff, U.; Mihaylov, L.; Spassov, T. The Mechanism of Generating Nanoporous Au by De-Alloying Amorphous Alloys. *Acta Mater.* **2016**, *119*, 177–183. [[CrossRef](#)]
14. Scaglione, F.; Celegato, F.; Rizzi, P.; Battezzati, L. A Comparison of De-Alloying Crystalline and Amorphous Multicomponent Au Alloys. *Intermetallics* **2015**, *66*, 82–87. [[CrossRef](#)]
15. Scaglione, F.; Xue, Y.; Celegato, F.; Rizzi, P.; Battezzati, L. Amorphous Molybdenum Sulphide @ Nanoporous Gold as Catalyst for Hydrogen Evolution Reaction in Acidic Environment. *J. Mater. Sci.* **2018**, *53*, 12388–12398. [[CrossRef](#)]
16. Xue, Y.; Scaglione, F.; Rizzi, P.; Battezzati, L.; Denis, P.; Fecht, H.-J. Electrodeposited Platinum on De-Alloyed Nanoporous Gold with Enhanced Electro-Catalytic Performance. *Appl. Surf. Sci.* **2019**, *476*, 412–417. [[CrossRef](#)]
17. Paschalidou, E.M.; Scaglione, F.; Gebert, A.; Oswald, S.; Rizzi, P.; Battezzati, L. Partially and Fully De-Alloyed Glassy Ribbons Based on Au: Application in Methanol Electro-Oxidation Studies. *J. Alloys Compd.* **2016**, *667*, 302–309. [[CrossRef](#)]
18. Ding, Y.; Chen, M. Nanoporous Metals for Catalytic and Optical Applications. *MRS Bull.* **2009**, *34*, 569–576. [[CrossRef](#)]
19. Sharma, B.; Frontiera, R.R.; Henry, A.I.; Ringe, E.; Van Duyne, R.P. SERS: Materials, Applications, and the Future. *Mater. Today* **2012**, *15*, 16–25. [[CrossRef](#)]
20. Schlücker, S. Surface-Enhanced Raman Spectroscopy: Concepts and Chemical Applications. *Angew. Chem.-Int. Ed.* **2014**, *53*, 4756–4795. [[CrossRef](#)]
21. Tian, Y.; Liu, H.; Zhao, G.; Tatsuma, T. Shape-Controlled Electrodeposition of Gold Nanostructures. *J. Phys. Chem. B* **2006**, *110*, 23478–23481. [[CrossRef](#)]
22. Zhou, Q.; Li, Z.; Yang, Y.; Zhang, Z. Arrays of Aligned, Single Crystalline Silver Nanorods for Trace Amount Detection. *J. Phys. D Appl. Phys.* **2008**, *41*, 152007. [[CrossRef](#)]
23. Chalmers, J.M.; Griffiths, P.R. *Handbook of Vibrational Spectroscopy*; John Wiley & Sons: Hoboken, NJ, USA, 2001; Volume 1. [[CrossRef](#)]
24. Morton, S.M.; Silverstein, D.W.; Jensen, L. Theoretical Studies of Plasmonics Using Electronic Structure Methods. *Chem. Rev.* **2011**, *111*, 3962–3994. [[CrossRef](#)] [[PubMed](#)]
25. Pieczonka, N.P.W.; Aroca, R.F. Single Molecule Analysis by Surface-Enhanced Raman Scattering. *Chem. Soc. Rev.* **2008**, *37*, 946–954. [[CrossRef](#)]
26. Zhang, L.; Liu, H.; Chen, L.; Guan, P.; Chen, B.; Fujita, T.; Yamaguchi, Y.; Iwasaki, H.; Xue, Q.-K.; Chen, M. Large-Scale Growth of Sharp Gold Nano-Cones for Single-Molecule SERS Detection. *RSC Adv.* **2016**, *6*, 2882–2887. [[CrossRef](#)]
27. Lim, D.-K.; Jeon, K.-S.; Hwang, J.-H.; Kim, H.; Kwon, S.; Suh, Y.D.; Nam, J.-M. Highly Uniform and Reproducible Surface-Enhanced Raman Scattering from DNA-Tailorable Nanoparticles with 1-Nm Interior Gap. *Nat. Nanotechnol.* **2011**, *6*, 452–460. [[CrossRef](#)] [[PubMed](#)]
28. Scaglione, F.; Paschalidou, E.M.; Rizzi, P.; Bordiga, S.; Battezzati, L. Nanoporous Gold Obtained from a Metallic Glass Precursor Used as Substrate for Surface-Enhanced Raman Scattering. *Philos. Mag. Lett.* **2015**, *95*, 474–482. [[CrossRef](#)]
29. Xue, Y.; Scaglione, F.; Rizzi, P.; Battezzati, L. High Performance SERS on Nanoporous Gold Substrates Synthesized by Chemical De-Alloying a Au-Based Metallic Glass. *Appl. Surf. Sci.* **2017**, *426*, 1113–1120. [[CrossRef](#)]
30. Scaglione, F.; Rizzi, P.; Celegato, F.; Battezzati, L. Synthesis of Nanoporous Gold by Free Corrosion of an Amorphous Precursor. *J. Alloys Compd.* **2014**, *615*, S142–S147. [[CrossRef](#)]
31. Xiao, S.; Xiao, F.; Hu, Y.; Yuan, S.; Wang, S.; Qian, L.; Liu, Y. Hierarchical Nanoporous Gold-Platinum with Heterogeneous Interfaces for Methanol Electrooxidation. *Sci. Rep.* **2014**, *4*, 4370. [[CrossRef](#)]
32. Lukaszewski, M.; Soszko, M.; Czerwiński, A. Electrochemical Methods of Real Surface Area Determination of Noble Metal Electrodes—An Overview. *Int. J. Electrochem. Sci.* **2016**, *11*, 4442–4469. [[CrossRef](#)]

33. Zhang, L.; Chen, L.; Liu, H.; Hou, Y.; Hirata, A.; Fujita, T.; Chen, M. Effect of Residual Silver on Surface-Enhanced Raman Scattering of Dealloyed Nanoporous Gold. *J. Phys. Chem. C* **2011**, *115*, 19583–19587. [[CrossRef](#)]
34. Nishio, K.; Masuda, H. Anodization of Gold in Oxalate Solution to Form a Nanoporous Black Film. *Angew. Chem.-Int. Ed.* **2011**, *50*, 1603–1607. [[CrossRef](#)] [[PubMed](#)]
35. Xu, S.; Yao, Y.; Wang, P.; Yang, Y.; Xia, Y.; Liu, J.; Li, Z.; Huang, W. Anodic Fabrication of Nanoporous Gold Films from Pure Gold in Oxalic Acid Solution and Their Applications in Electrocatalysis and Sers. *Int. J. Electrochem. Sci.* **2013**, *8*, 1863–1870.
36. Ocean Optics SERS Substrates Surface Enhanced Raman Spectroscopy. Available online: www.oceanoptics.com (accessed on 20 March 2020).
37. Hamamatsu SERS Substrate That Enhances the Weak Raman Scattered Light from the Molecu. Available online: <https://www.hamamatsu.com/jp/en/product/type/J12853/index.html> (accessed on 20 March 2020).
38. Ngai, K.S.; Tan, W.T.; Zainal, Z.; Zawawi, R.B.M.; Zidan, M. Electrochemical Oxidation of Ascorbic Acid Mediated by Single-Walled Carbon Nanotube/Tungsten Oxide Nanoparticles Modified Glassy Carbon Electrode. *Int. J. Electrochem. Sci.* **2012**, *7*, 4210–4222.
39. Joo, S.W. Surface-Enhanced Raman Scattering of 4,4'-Bipyridine on Gold Nanoparticle Surfaces. *Vib. Spectrosc.* **2004**, *34*, 269–272. [[CrossRef](#)]
40. Suzuki, M.; Niidome, Y.; Yamada, S. Adsorption Characteristics of 4,4'-Bipyridine Molecules on Gold Nanosphere Films Studied by Surface-Enhanced Raman Scattering. *Thin Solid Film.* **2006**, *496*, 740–747. [[CrossRef](#)]
41. Huang, J.; Chen, F.; Zhang, Q.; Zhan, Y.; Ma, D.; Xu, K.; Zhao, Y. 3D Silver Nanoparticles Decorated Zinc Oxide/Silicon Heterostructured Nanomace Arrays as High-Performance Surface-Enhanced Raman Scattering Substrates. *ACS Appl. Mater. Interfaces* **2015**, *7*, 5725–5735. [[CrossRef](#)]
42. Zhang, X.; Xiao, X.; Dai, Z.; Wu, W.; Zhang, X.; Fu, L.; Jiang, C. Ultrasensitive SERS Performance in 3D “Sunflower-like” Nanoarrays Decorated with Ag Nanoparticles. *Nanoscale* **2017**, *9*, 3114–3120. [[CrossRef](#)]
43. Zhang, L.; Lang, X.; Hirata, A.; Chen, M. Wrinkled Nanoporous Gold Films with Ultrahigh Surface-Enhanced Raman Scattering Enhancement. *ACS Nano* **2011**, *5*, 4407–4413. [[CrossRef](#)]
44. Xue, Y.; Scaglione, F.; Paschalidou, E.M.; Rizzi, P.; Battezzati, L. Excellent Surface Enhanced Raman Scattering Obtained with Nanoporous Gold Fabricated by Chemical De-Alloying. *Chem. Phys. Lett.* **2016**, *665*, 6–9. [[CrossRef](#)]
45. Federico, S.; Rizzi, P.; Battezzati, L. METODO PER LA PREPARAZIONE DI ORO NANOPOROSO ANODIZZATO, ORO NANOPOROSO ANODIZZATO E SUOI. USI. Patent number 10202000024382, 15 October 2020.
46. Federico, S.; Rizzi, P.; Battezzati, L. METODO PER LA PREPARAZIONE DI ORO NANOPOROSO ANODIZZATO, ORO NANOPOROSO ANODIZZATO E SUOI. USI. Patent number PCT/IB2021/059525, 15 October 2021.